# Spatially coordinated collective phosphorylation filters spatiotemporal noises for precise circadian timekeeping

Seok Joo Chae[1,2], Dae Wook Kim[3], Seunggyu Lee[2,4], Jae Kyoung Kim[1,2,5,*]

[1] Department of Mathematical Sciences, Korea Advanced Institute of Science and Technology, Daejeon, 34141, Republic of Korea

[2] Biomedical Mathematics Group, Institute for Basic Science, Daejeon, 34126, Republic of Korea

[3] Department of Mathematics, University of Michigan, Ann Arbor, MI, 48109, USA

[4] Division of Applied Mathematical Science, Korea University, Sejong, 30019, Republic of Korea

[5] Lead Contact

*Correspondence: jaekkim@kaist.ac.kr

# Graphical Abstract

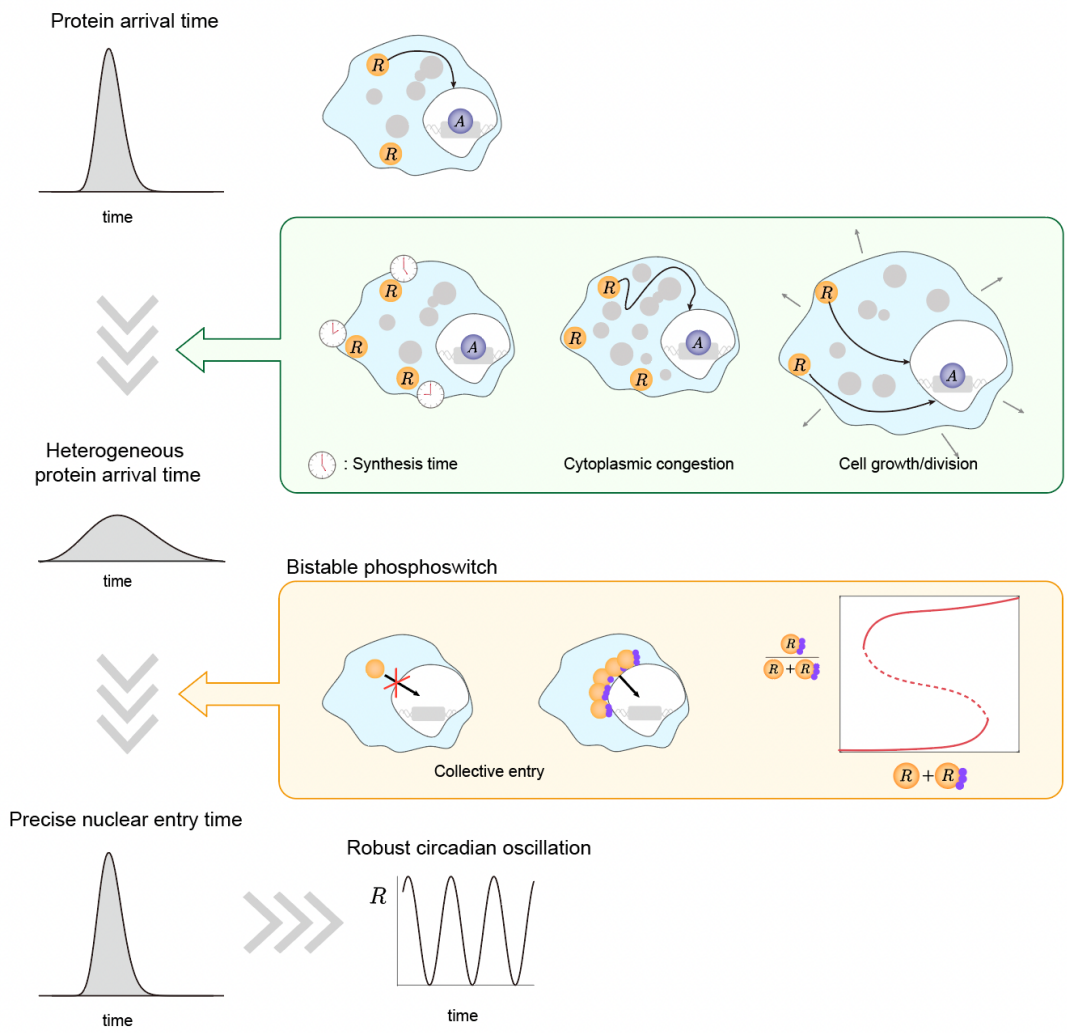


# Highlights

- The time window when PER protein arrives at the perinucleus is wide and keeps changing.
- A bistable phosphoswitch enables precise nuclear entry of PER protein.
- This leads to robust circadian rhythms when cell congestion level and size change.
- This describes how the circadian clock compensates for spatiotemporal noise.

## Summary

The circadian (~24h) clock is based on a negative feedback loop centered around the PERIOD protein (PER), translated in the cytoplasm and then enters the nucleus to repress its own transcription at the right time of day. Such precise nucleus entry is mysterious because thousands of PER molecules transit through crowded cytoplasm and arrive at the perinucleus across several hours. To understand this, we developed a mathematical model describing the complex spatiotemporal dynamics of PER as a single random time delay. We find that the spatially coordinated bistable phosphoswitch of PER, which triggers the phosphorylation of accumulated PER at the perinucleus, leads to the synchronous and precise nuclear entry of PER. This leads to robust circadian rhythms even when PER arrival times are heterogenous and perturbed due to changes in cell crowdedness, cell size, and transcriptional activator levels. This shows how the circadian clock compensates for spatiotemporal noise.

## Introduction

The mammalian circadian (~24h) clock is a self-sustained endogenous oscillator that relies on a transcriptional-translational negative feedback loop (TTFL), where the activator complex, BMAL1:CLOCK, promotes the transcription of *Per1/2* and *Cry1/2* genes, and the PER:CRY complex inhibits BMAL1:CLOCK to close the loop[1-6]. In the TTFL, precise transcriptional repression (i.e., transcription being repressed at the right time of the day) of BMAL1:CLOCK by the PER complex is essential to generate circadian rhythms[7-10].

However, obtaining such precise transcriptional repression is challenging because individual PER molecules are expected to arrive at the perinucleus at different times. Specifically, thousands of PER molecules transit through the crowded intracellular environment with organelles and macromolecules, leading to different travel times for each PER molecule. Moreover, since the cell size keeps changing due to cell growth and cell division, the travel distance of PER molecules to the perinucleus also keeps changing. The heterogeneity in the PER arrival time is further amplified as PER molecules are translated across several hours at different places[8,11,12]. Furthermore, the amount of activator proteins of the transcription (e.g., BMAL1), which promotes the production of PER protein, also exhibits a noisy fluctuation with daily changes[13,14]. As a result, the arrival time of PER molecules largely varies during a single day and exhibits daily variations. Interestingly, although thousands of PER molecules arrive at the perinucleus across several hours, they enter the nucleus during a narrow time window at the right time every day[8], leading to transcriptional repression with precise timing, and thus to robust circadian rhythms. This indicates the existence of some mechanism that filters the heterogeneity in the protein arrival time.

This filtering mechanism has barely been investigated. Even the widely used mathematical models of the circadian clock assume that PER is homogenously distributed in the cytoplasm, and thus they are not able to capture the cytoplasmic trafficking of PER[15-31]. Notably, it has been shown that when the cytoplasmic trafficking of Hes1 molecules is incorporated into a mathematical model, the period of Hes1 oscillation greatly changes (~three-fold)[32]. This indicates that the variability in the protein arrival time distribution should be filtered to generate stable rhythms. Previously, a

75 potential filtering mechanism was proposed: If traveling molecules degrade quickly
76 enough, molecules that spend a long time during cytoplasmic trafficking are degraded
77 before they arrive at the perinucleus[33], and thus only molecules traveling along optimal
78 paths enter the nucleus without being degraded. Although this results in a narrow
79 distribution of nuclear entry time, it requires an unrealistically short half-life of proteins (on
80 the order of 1ms)[34]. Recently, a biologically feasible filtering mechanism, the spatially
81 coordinated bistable phosphoswitch of PER, was suggested[8]. That is, when enough PER
82 molecules are accumulated in the perinucleus, the bistable switch-like phosphorylation of
83 PER is triggered. As a result, PER molecules at the perinucleus are synchronously
84 phosphorylated, which is necessary for their nuclear entry, and enter the nucleus together.
85 This allows thousands of PER molecules that arrive at the perinucleus at different times
86 to enter the nucleus within a narrow time window. However, such filtering effect was
87 investigated only under an ideal condition that does not include critical factors that affect
88 the protein arrival time, such as variation in cytoplasmic congestion level, cell size, and
89 activator amount.

90 Here, we investigated whether the bistable phosphoswitch of PER can filter the
91 variability in its arrival time distribution under various noise sources: different cytoplasmic
92 congestion levels, cell sizes, and activator amounts. Specifically, we developed a
93 stochastic model simulating the TTFL of PER, where the PER travel time to the
94 perinucleus is described by a time delay distribution. Thus, changing the delay
95 parameters allows us to effectively describe the change in the travel time due to the
96 variation in cytoplasmic congestion and cell size. Using the framework, we found that
97 bistable phosphorylation of PER can effectively filter the heterogeneity in PER arrival time,

resulting in precise repression timing and robust circadian rhythms. On the other hand, such filtering does not occur when PER phosphorylation occurs via conventional phosphorylation mechanisms, such as linear and ultrasensitive phosphorylations. Furthermore, by integrating our model with a previously measured BMAL1 time series in a single cell[14], we showed that bistable phosphorylation can lead to the precise timing of nuclear entry and robust circadian rhythms even under the large intra- and inter-daily variation in the amount of the activator proteins. Taken together, the bistable phosphoswitch for nuclear entry can filter heterogeneity in protein arrival time and lead to robust rhythms under diverse environments. Our approach sets the stage for systematically exploring how the circadian clock can filter diverse spatiotemporally generated noises in the cell to generate robust circadian rhythms.

# Results

**Synchronous nuclear entry of PER molecules compensates for their spatiotemporal heterogeneity and leads to robust circadian rhythms.**

In the TTFL of the mammalian circadian clock, the translated PER protein at the cytoplasm ($R_c$) approaches the perinucleus while it forms a complex with CRY proteins and CK1$\delta/\epsilon$ ($R_p$), and it is phosphorylated at multiple sites (Figure 1A)[35-39]. Then, the phosphorylated PER complex in the perinucleus ($R_p'$) can enter the nucleus, where the PER complex ($R_n$) represses its own transcriptional activator ($A$). The time it takes for PER protein to reach the perinucleus ($\tau$) is affected by various biological factors such as cell size (Figure 1B), congestion level (Figure 1C), and the mode of PER transport toward the nucleus (Figure 1D).

121 To quantitatively study how $\tau$ varies due to these factors, we used an agent-based
122 model that simulates the movement of individual PER molecules from the cell membrane
123 to the perinucleus (see Supplementary Information for details). The movement of PER
124 can be either purely diffused, with a random direction, or directed towards the nucleus in
125 the model. When PER is purely diffused, we used the experimentally measured diffusion
126 coefficient[11,12]. As the advection probability increases, the travel time of PER toward the
127 perinucleus ($\tau$) becomes shorter (Figure S1). Thus, as the advection probability increases,
128 we decreased the diffusion coefficient so that the mean of $\tau$ ($\mu_\tau$) is maintained. For the
129 simulation, we used the cell size obtained from the average of a mouse fibroblast cell
130 population distribution ($\mu_A$)[40] (Figure 1E) (see Supplementary Information for details). We
131 also increased or decreased the cell size by the standard deviation of the distribution ($\sigma_A$)
132 to investigate the effect of cell size on $\tau$. Furthermore, to consider the effect of congestion
133 level, we also introduced obstacles in the cytoplasm, slowing down the movement of PER,
134 with varying numbers (i.e., different levels of crowdedness).

135 As cell size increases (left to right, Figure 1F) or crowdedness increases (blue to
136 yellow, Figure 1F), the travel time to reach the perinucleus ($\tau$) becomes longer and less
137 precise, i.e., both the mean ($\mu_\tau$) and standard deviation ($\sigma_\tau$) of the time delay increase.
138 As the chance of advection increases (top to bottom Figure 1F), $CV_\tau$ decreases, indicating
139 a more precise arrival time with advection compared to diffusion. However, even with
140 strong advection, the distribution of $\tau$ remains quite wide and becomes wider as a cell
141 grows and becomes more crowded. Note that the distribution is obtained under the
142 assumption that PER proteins are translated at the same time and the same location.
143 Thus, the distribution of PER arrival times at the perinucleus ($t_p$) is expected to be even

144 more heterogeneous because PER proteins are translated at different places in the
145 cytoplasm over several hours, leading to different travel distances and departure times,
146 respectively[8,11,12]. If $R_p'$ enters the nucleus in the order of arrival at the perinucleus,
147 nuclear entry occurs within a wide time window (i.e., the distribution of $t_n$ is wide) (Figure
148 1G (ii), green), and thus transcriptional activity decreases gradually (Figure 1G (iii), green),
149 weakening the circadian rhythms (Figure 1G (iv), green)[41-43]. Therefore, to generate
150 strong circadian rhythms, a mechanism narrowing the distribution of $t_n$ is required (Figure
151 1G, red). The presence of such a filtering mechanism is supported by the distribution of
152 circadian periods across a mouse fibroblast cell population. Specifically, since these cells
153 have highly variable sizes (mean $\pm$ SD, 2346 $\pm$ 558 $\mu m^2$; CV=24%) (Figure 1E)[40],
154 individual cells are expected to have varying protein travel time distributions. Indeed, the
155 calculated distribution of $\mu_\tau$ across the fibroblast population with a partial differential
156 equation equivalent to the ABM is highly variable (mean ± SD of 5.12 ± 1.94 h) (Figure
157 1H) (see Supplementary Information for details). However, compared to the variation in
158 travel times, the variation in the circadian periods of the mouse fibroblast cells with
159 different sizes was much smaller (mean ± SD of 22.97 ± 0.91h) (Figure 1H). This indicates
160 the presence of a mechanism to filter the heterogeneous cytoplasmic trafficking time ($\tau$)
161 to generate similar circadian periods across different cell sizes. Such a mechanism is
162 expected to be based on the phosphorylation mechanism of $R_p$ because $R_p$ can enter the
163 nucleus only after phosphorylation[3,35,44].
164

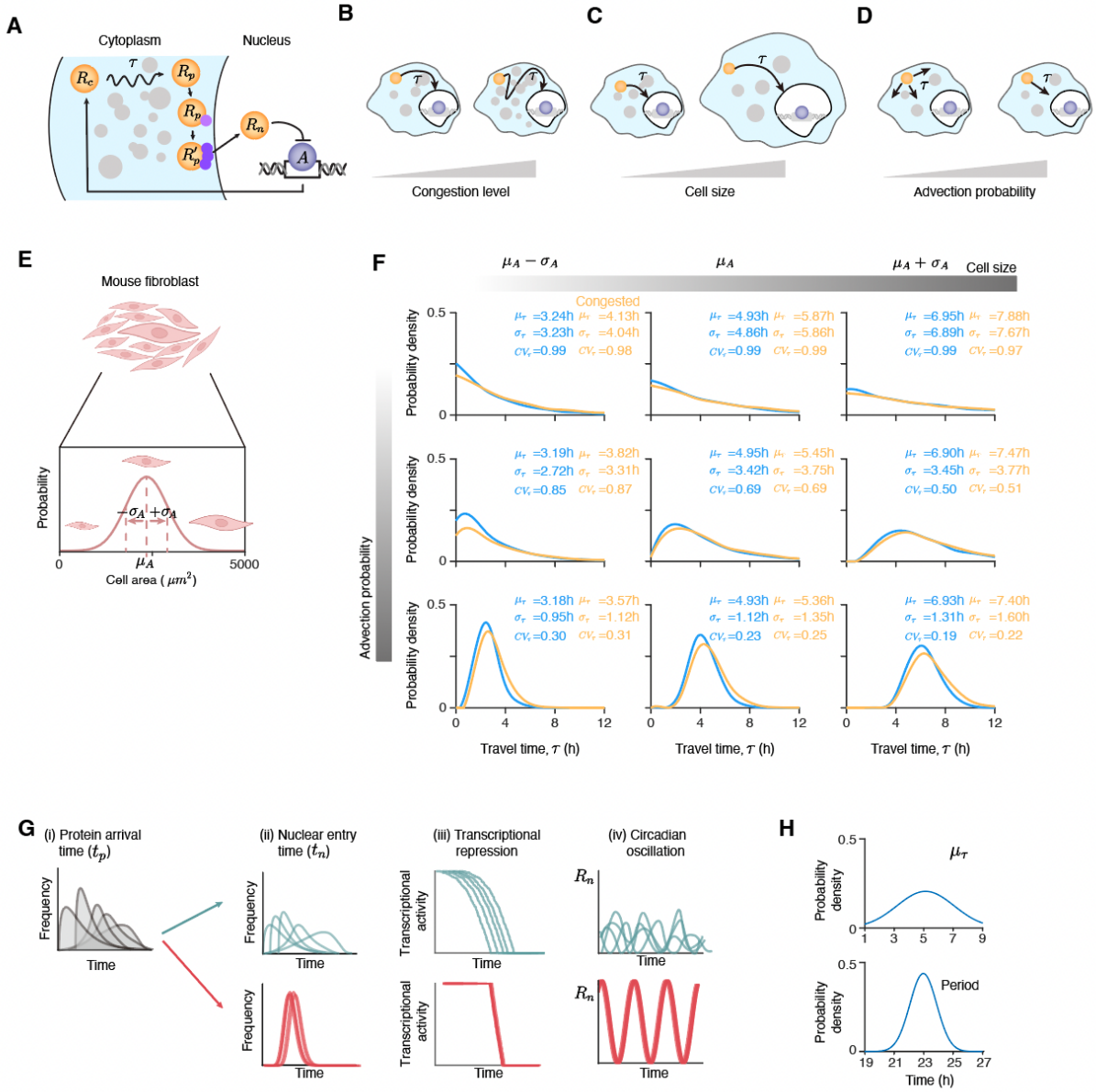


165

166 **Figure 1. Precise timing of repression is required to generate robust circadian**
167 **rhythms in various environments. (A)** Schematic diagram of the circadian clock model.
168 PER protein is synthesized in the cytoplasm ($R_c$), and then it transits toward the
169 perinucleus while it forms a complex with CRY and CK1$\delta/\varepsilon$ ($R_p$), and it undergoes
170 multisite phosphorylation. After being phosphorylated, PER complex in the perinucleus
171 ($R'_p$) can enter the nucleus ($R_n$) to inhibit its own transcriptional activator ($A$). $R_c$ passes
172 through a cytoplasm, and then arrives at the perinucleus after the travel time $\tau$. **(B-D)** The
173 travel time $\tau$ changes as the crowdedness of cells (B), the size of cells (C) and the chance
174 of advection toward the nucleus (D) change. **(E)** Mouse fibroblast cell size is highly
175 variable, having a mean $\pm$ SD, 2346 $\pm$ 558 $\mu m^2$ (CV=24%)[40]. Thus, the travel time ($\tau$) is

expected to be highly variable from cell to cell. **(F)** The distribution of travel time ($\tau$) varies greatly depending on cytoplasmic congestion level, cell size, and advection probability. As the cell size increases, $\mu_\tau$ and $\sigma_\tau$ increase. Similarly, a congested cell (yellow) has higher $\mu_\tau$ and $\sigma_\tau$ than a less congested cell (blue). Increasing advection probability while retaining the same $\mu_\tau$ leads to a decrease in $CV_\tau$. **(G)** Due to the various travel times ($\tau$) and the synthesis of proteins over several hours, the arrival time of proteins at the perinucleus ($t_p$) is highly variable. Without a filtering mechanism, the distribution of nuclear entry time ($t_n$) also becomes wide (green line, (ii)), leading to a gradual decline of transcriptional activity (green line, (iii)), and thus weak circadian rhythms (green line, (iv)). A filtering mechanism narrowing the distribution of $t_n$ (red line, (ii)) is needed for sharp transcriptional repression (red line, (iii)), and thus robust circadian rhythms (red line, (iv)). **(H)** Indeed, for mouse fibroblast cells with different sizes[40], compared to the distribution of mean travel time, the distribution of circadian periods is much narrower, indicating the presence of a noise filtering mechanism.

**Bistable phosphorylation of PER is required to enter the nucleus in the circadian clock.**

PER protein has multiple CK1-dependent phosphorylation sites where the phosphorylation of these sites occurs in a cooperative manner[8,45]. As a result, the phosphorylation occurs collectively, i.e., the phosphorylation is affected by the local concentration of the PER complex (Figure 2A, red)[8]. Specifically, when the local concentration of the PER complex is lower than the switch-on threshold (Figure 2A, black triangle), phosphorylation does not occur. However, once the local concentration reaches the switch-on threshold, the majority of the PER complex is synchronously phosphorylated, resulting in a sharp increase in the phosphorylated fraction. Furthermore, the high fraction of phosphorylated PER complex persists for awhile, even after the local concentration decreases below the switch-on threshold, until it reaches the switch-off threshold (Figure 2A, gray triangle). To investigate the advantage of having such bistable phosphorylation of $R_p$ in reducing the heterogeneity in the distribution of $t_n$, we compare

it with the other typical phosphorylation mechanisms: ultrasensitive phosphorylation and linear phosphorylation. Ultrasensitive phosphorylation also has a switch-on threshold for synchronous phosphorylation, similar to bistable phosphorylation, but it does not have a distinct switch-off threshold (Figure 2A, blue)[43,46]. Thus, the fraction of the $R_p'$ monotonically increases as the total amount of PER in the perinucleus increases, with the sigmoidal pattern having a steep increase near the switch-on threshold. In linear phosphorylation, the fraction of the $R_p'$ is constant (Figure 2A, green): only the fixed portion of the PER complex is phosphorylated regardless of the local concentration of PER complex.

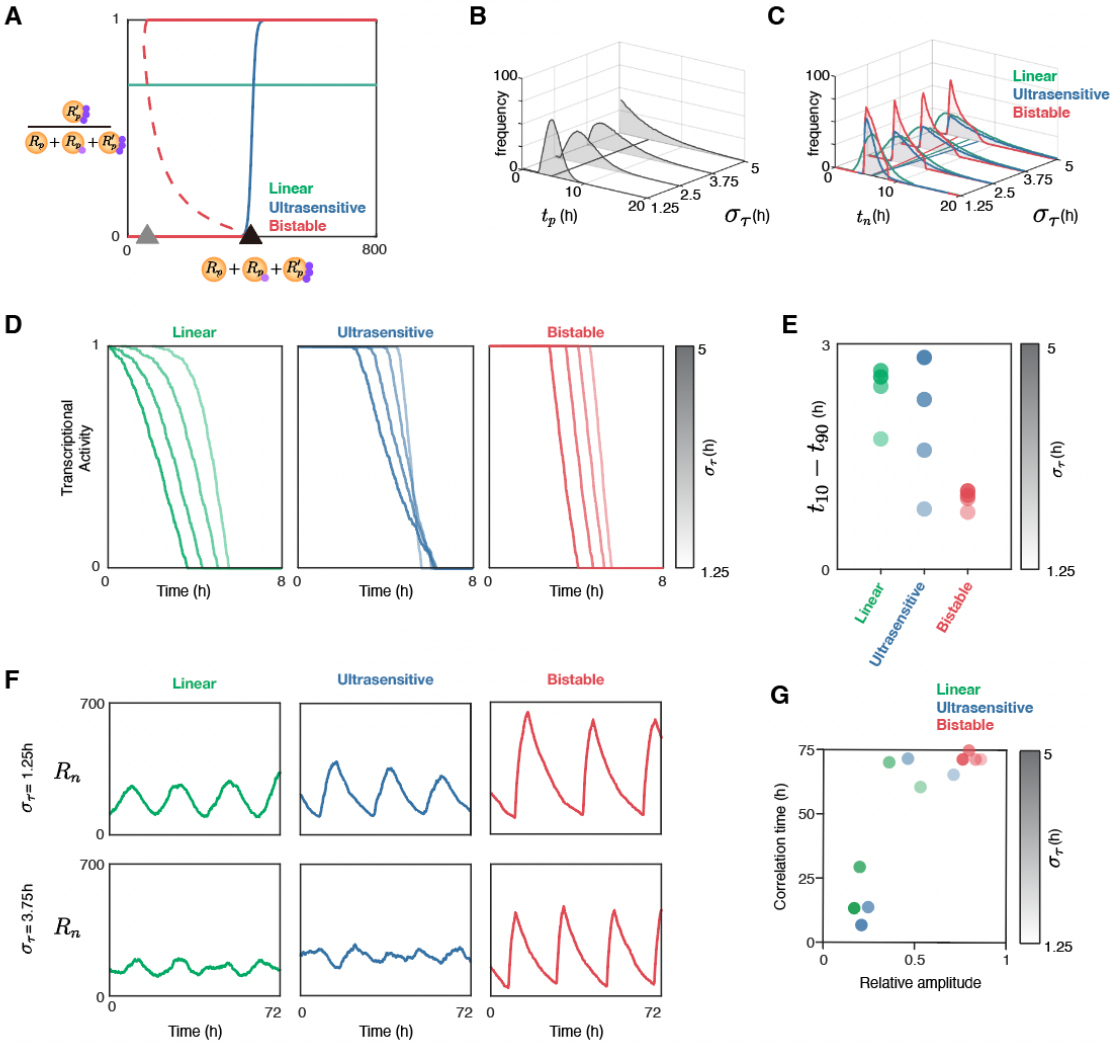


**Figure 2. Spatially coordinated collective phosphorylation of PER proteins leads to robust circadian oscillations under noisy protein arrival. (A)** Three representative phosphorylation mechanisms for nuclear entry. In linear phosphorylation, the fraction of $R_p'$ is the same regardless of the local concentration of the total PER complex in the perinucleus. In ultrasensitive and bistable phosphorylations, the fraction of $R_p'$ steeply increases when the local concentration of the total PER complex reaches the switch-on threshold (black triangle). With bistable phosphorylation, the fraction of $R_p'$ persists even when the local concentration of the total PER complex decreases below the switch-on threshold until the local concentration of the total PER complex reaches the switch-off threshold (gray triangle). **(B-C)** As the protein travel time becomes noisy (i.e., $\sigma_\tau$ increases), thousands of PER molecules arrive at the perinucleus within a wide time window ($t_p$). As a result, the distribution of nuclear entry time ($t_n$) also becomes significantly wider with linear (green) or ultrasensitive (blue) phosphorylation, but not with bistable phosphorylation (red). Here, the distributions were obtained from 200 repeated

229 simulations. **(D)** As $\sigma_\tau$ increases (light to dark colors), with linear and ultrasensitive
230 phosphorylations, transcriptional activity decreases gradually (green and blue). In
231 contrast, with bistable phosphorylation, transcriptional activity decreases sharply
232 regardless of $\sigma_\tau$ (red). **(E)** The sensitivity of transcription repression is quantified by
233 measuring the time taken for the transcriptional activity to decrease from 90% ($t_{90}$) to 10%
234 of the maximal transcriptional activity ($t_{10}$). The smaller value of $t_{10} - t_{90}$ indicates the
235 sharper repression of transcription. **(F)** Robust oscillations are maintained with bistable
236 phosphorylation even under noisy cytoplasmic trafficking (i.e., high $\sigma_\tau$), but not with linear
237 and ultrasensitive phosphorylations. **(G)** The robustness of the oscillations was quantified
238 by the correlation time and the relative amplitude of $R_n$ oscillatory time series. The longer
239 correlation time indicates the more robust oscillation.
240
241
242 **Bistable phosphorylation of PER allows sharp transcriptional repression despite**
243 **the heterogeneous PER arrival times at the perinucleus.**

244 We compared how the distribution of nuclear entry times ($t_n$) is affected as the
245 variance in the arrival time ($t_p$) increases depending on the three phosphorylation
246 mechanisms regulating nuclear entry. For this, we constructed a mathematical model
247 which describes part of the TTFL (Figure 1A): the cytoplasmic trafficking of $R_c$ to $R_p$, the
248 phosphorylation of $R_p$ to $R_p'$, and the nuclear entry of $R_p'$ to $R_n$ (see STAR Methods for
249 detailed model descriptions and Table S1 for the propensity functions of reactions). To
250 focus on how phosphorylation affects the distribution of $t_n$, we assumed that PER
251 molecules are not degraded. Additionally, the time spent during the cytoplasmic trafficking
252 was assumed to be gamma distributed, because the distributions of $\tau$ in Figure 1F
253 approximately follow the gamma distribution. After arrival at the perinucleus, $R_p$
254 undergoes phosphorylation with one of the three phosphorylation mechanisms (Figure
255 2A) and enters the nucleus. We assumed that $R_p$ stays at the perinucleus and that the
256 phosphorylation of the PER protein only occurs at the perinucleus, based on a previous
257 study[8], which observed the enrichment of the PER protein and phosphorylation mainly at

258 the perinucleus. To describe the different types of phosphorylation, we adopted the
259 modular approach, which describes complex multistep reactions with a single
260 phenomenological module that qualitatively describes the dynamical behavior[46,47]. This
261 allowed us to simulate the complex phosphorylation process, which is necessary for
262 nuclear entry (see STAR Methods for details). We simulated the situation where 1,000
263 PER complexes travel from the cell membrane to the perinucleus using the delayed
264 Gillespie algorithm[48,49]. This allowed us to calculate the time when each $R_c$ arrives at the
265 perinucleus ($t_p$) and then when it enters the nucleus ($t_n$). In this way, we obtained the
266 distribution of $t_p$ and $t_n$ of the 1,000 PER complexes, which quantifies the heterogeneity
267 in the protein arrival time and the nuclear entry time, respectively.

268 As we increase the standard deviation of the travel time ($\sigma_\tau$) while keeping its mean
269 ($\mu_\tau$) constant, the distribution of $t_p$ becomes wider (Figure 2B). As a result, the distribution
270 of $t_n$ also becomes wider with linear and ultrasensitive phosphorylations (Figure 2C,
271 green and blue), and thus transcriptional activity decreases gradually (Figure 2D, green
272 and blue). However, the narrow distribution of $t_n$ is maintained with bistable
273 phosphorylation (Figure 2C, red), and thus transcriptional repression occurs sharply
274 regardless of the $\sigma_\tau$ (Figure 2D, red). To quantify the sensitivity of the transcriptional
275 repression (i.e., how rapidly the transcriptional activity is decreased), the difference
276 between the time when the transcriptional activity reaches 10% of the maximal
277 transcriptional activity ($t_{10}$) and the time when the transcriptional activity reaches 90% of
278 the maximal transcriptional activity ($t_{90}$) was calculated. With bistable phosphorylation,
279 $t_{10} - t_{90}$ is small (i.e., sharp repression) regardless of $\sigma_\tau$ (Figure 2E). On the other hand,
280 with linear and ultrasensitive phosphorylations, $t_{10} - t_{90}$ greatly increases as

281 $\sigma_\tau$ increases. This indicates that bistable phosphorylation, but not linear and ultrasensitive
282 phosphorylations, allows sharp transcriptional repression even when the protein arrives
283 at the perinucleus with heterogeneous timing (i.e., the variance of $t_p$ is large.)
284

285 **Robust circadian rhythms can be generated even with highly variable travel time**
286 **through bistable phosphorylation.**

287 In the previous section, to focus on the nuclear entry time ($t_n$) of $R_p'$, we used a
288 model describing part of the TTFL (Figure 1A). Now, we have extended the model to fully
289 describe the TTFL. Specifically, in the model, the transcriptional activator ($A$) is
290 suppressed by $R_n$ via protein sequestration[19,21,22,28], which closes the negative feedback
291 loop. Furthermore, the degradations of $R_c, R_p, R_p'$, and $R_n$ were also incorporated into the
292 model. With this model, we investigated how the noise level in the travel time (i.e., $\sigma_\tau$)
293 affects circadian rhythms. As $\sigma_\tau$ increases, the simulated oscillations of $R_n$ become noisy
294 with linear and ultrasensitive phosphorylations (Figure 2F, green and blue). On the other
295 hand, even when $\sigma_\tau$ increases, robust oscillations are maintained with bistable
296 phosphorylation (Figure 2F, red). To quantify the accuracy and the strength of the
297 simulated oscillations, we calculated the correlation time and the relative amplitude of the
298 time series of $R_n$ (see STAR Methods). The correlation time describes how fast the
299 autocorrelation function of the oscillatory time series decays[50,51]. If the time series exhibits
300 a noisy oscillation, autocorrelation will decay rapidly, resulting in a short correlation time.
301 The correlation time becomes short and relative amplitude becomes small with linear and
302 ultrasensitive phosphorylations when $\sigma_\tau$ increases (Figure 2G, green and blue). In other
303 words, linear and ultrasensitive phosphorylations become less likely to generate rhythms

304 as $\sigma_\tau$ increases. This result is consistent with a previous study[52], which showed that
305 negative-feedback oscillators find it challenging to generate rhythms with a distributed
306 delay that has a large width. On the other hand, the correlation time is long and the relative
307 amplitude is large regardless of $\sigma_\tau$ with bistable phosphorylation (Figure 2G, red). Taken
308 together, with bistable phosphorylation, robust oscillations can be generated even when
309 $\sigma_\tau$ is large.
310

311 **The effect of travel time on circadian periods is reduced by bistable**
312 **phosphorylation.**

313 Next, we examined if bistable phosphorylation can generate robust and precise
314 rhythms even when $\mu_\tau$ and $\sigma_\tau$ change simultaneously. For this, we simulated the TTFL
315 model used in Figures 2F and 2G for cells with different $\mu_\tau$ and $\sigma_\tau$. We used $\mu_\tau$ obtained
316 from 1,000 mouse fibroblast cells with different sizes (Figure 1H), and fixed $CV_\tau$ to be 0.5
317 so that $\sigma_\tau = 0.5 \cdot \mu_\tau$. As $\mu_\tau$ and $\sigma_\tau$ vary, bistable phosphorylation leads to a much
318 narrower distribution of periods (SD=1.97h) compared to linear and ultrasensitive
319 phosphorylations (SD=4.37h and SD=4.41h, respectively) (Figure 3A). Even when we
320 fixed $CV_\tau$ to different values (such as 0.25 or 0.75), we could obtain consistent results
321 (Figure S2). Thus, bistable phosphorylation generates robust and accurate rhythms when
322 both the mean ($\mu_\tau$) and the standard deviation ($\sigma_\tau$) vary.
323

324 We then investigated how bistable phosphorylation compensates for the effect of
325 change in $\mu_\tau$ and $\sigma_\tau$ on the circadian period. To do this, a model describing part of the
326 TTFL (Figures 2B and 2C) with different $\mu_\tau$ and $\sigma_\tau$ was utilzed. We used five

327 representatives of $\mu_\tau$ obtained from five cell areas: $\mu_A - 2\sigma_A$, $\mu_A - \sigma_A$, $\mu_A$, $\mu_A + \sigma_A$, *and*
328 $\mu_A + 2\sigma_A$ (Figures 1E and 1H top). We again set $\sigma_\tau = 0.5 \cdot \mu_\tau$ by fixing $CV_\tau \left(= \frac{\sigma_\tau}{\mu_\tau}\right)$ to 0.5
329 as in Figure 3A. We then examined how these various values of $\mu_\tau$ and $\sigma_\tau$, obtained from
330 five different cell areas, affected the nuclear entry time ($t_n$) under each phosphorylation
331 mechanism. As the cell size increases, and thus $\mu_\tau$ increases, the simulated time
332 trajectories of the nuclear entry propensity (Tables S1 and S2) are shifted to the right
333 (Figure 3B). Thus, the mean of nucleus entry time ($t_n$) increases for all three
334 phosphorylation mechanisms (Figure 3C), which is expected to lengthen the period.
335 Furthermore, as $\sigma_\tau$ also increases due to the cell size increase, PER molecules enter the
336 nucleus in a wider time window, and thus the time trajectories of the nuclear entry
337 propensity become wider and lower. Lower nuclear entry propensity results in a slow
338 increase in $R_n$ (Figure 3B), which may further lengthen the period. Interestingly, such
339 change is much smaller with bistable phosphorylation compared to linear and
340 ultrasensitive phosphorylation (Figure 3B). That is, the increase in the standard deviation
341 of $t_n$ is significantly larger with linear and ultrasensitive phosphorylations than with
342 bistable phosphorylation (Figure 3D). As a result, when the TTFL model was simulated
343 for each phosphorylation mechanism, the time between the minimum of $R_n$ and the
344 maximum of $R_n$ became longer (i.e., $R_n$ accumulated more slowly) in a larger cell with
345 linear and ultrasensitive phosphorylations, but not with bistable phosphorylation (Figure
346 3E). Specifically, the mean length of time during which $R_n$ increased more than two-fold
347 change varied from ~4h to ~10h as the cell area increased from $\mu_A - 2\sigma_A$ to $\mu_A + 2\sigma_A$ with
348 linear and ultrasensitive phosphorylations (Figure 3F, green and blue). On the other hand,
349 with bistable phosphorylation, the accumulation time of $R_n$ was nearly the same

regardless of the cell area (Figure 3F, red). This explains why the change in the circadian period due to the cell size variation is smaller with bistable phosphorylation than with other phosphorylation mechanisms (Figure 1H).

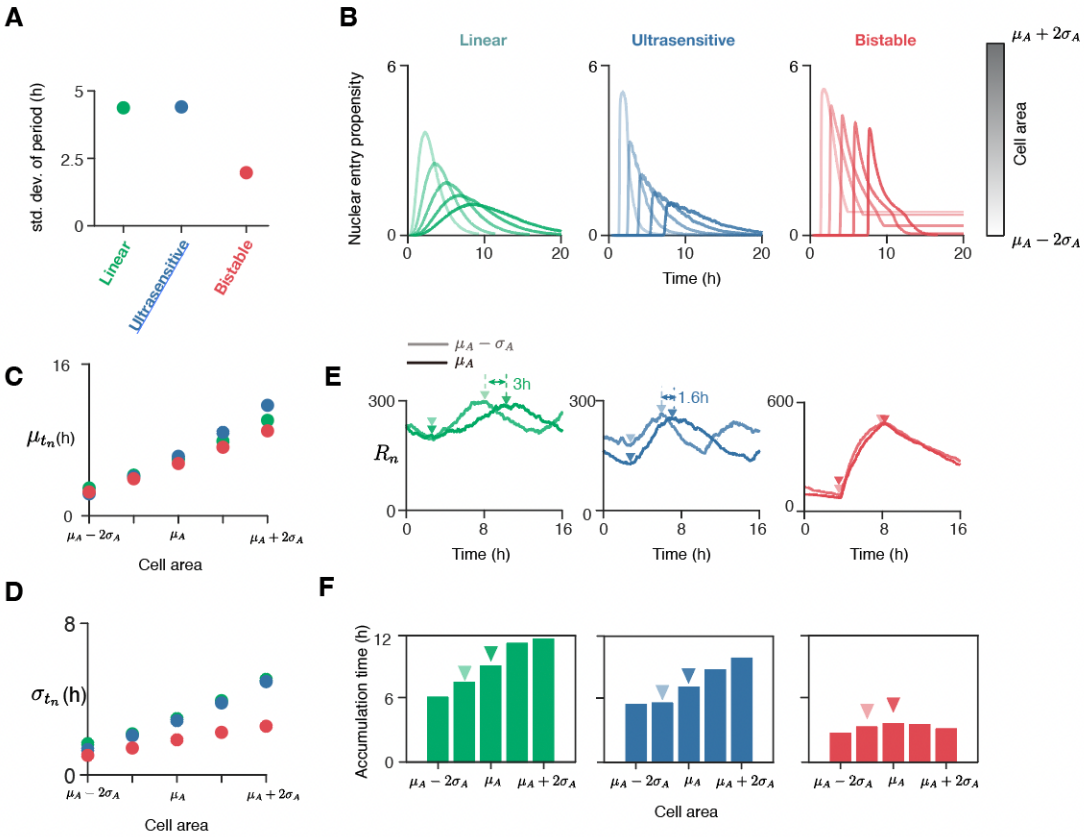


**Figure 3. Bistable phosphorylation enables cells of different sizes to have similar periods. (A)** For mouse fibroblast cells with different sizes[40], although the standard deviation of the mean ($\mu_\tau$) and the standard deviation ($\sigma_\tau$) of time spent during the cytoplasmic trafficking are ~2h, the standard deviation of the circadian periods is only a half of them (SD=0.91h). **(B)** The standard deviation of the simulated circadian periods for 1,000 cells, whose areas were sampled from the $N(2346\mu m^2,\ 558^2\mu m^4)$. **(C)** In a larger cell, $\mu_\tau$ and $\sigma_\tau$ increase. Thus, the time trajectories of the nuclear entry propensity (Tables S1 and S2) are shifted to the right and become wider. Note that with bistable phosphorylation, the nuclear entry occurs in a narrow time window, even in larger cells. The distributions were obtained with 200 repeated simulations. $\mu_A$ (=2346$\mu m^2$) and $\sigma_A$ (=558$\mu m^2$) are the mean and standard deviation of fibroblast cell area, respectively. **(D-E)** While the mean of the nuclear entry time ($\mu_{t_n}$) increases similarly in all three

367 phosphorylation mechanisms, bistable phosphorylation resulted in a far smaller standard
368 deviation in nuclear entry time ($\sigma_{t_n}$) than linear and ultrasensitive phosphorylations. **(F-G)**
369 As a result, the length of time during which $R_n$ accumulates from the trough (triangle) to
370 the peak (triangle) of $R_n$ does not change regardless of cell area with bistable
371 phosphorylation, but this is not the case with linear and ultrasensitive phosphorylations.
372

373 **Bistable phosphorylation enables robust circadian rhythms despite noisy activator**
374 **rhythms.**

375 In the previous sections, the amount of activator protein was assumed to be
376 constant over time. However, the amount of activator molecules, such as BMAL1,
377 oscillates with a period of ~24h[13,14,35,53] (Figure 4A). In addition, the amplitude and the
378 peak-to-peak period of BMAL1 protein fluctuate from day to day. Specifically, the
379 amplitude and the peak-to-peak period of experimentally measured BMAL1 proteins in a
380 single cell highly vary[14]: 286±35 and 25.4±5.7h (Figure 4A). Furthermore, an additional
381 'bump' often exists between the peaks. Due to the noisy pattern, it is expected that the
382 synthesis timing of PER will be heterogeneous, resulting in the heterogeneous protein
383 arrival time distribution. We investigated whether bistable phosphorylation enables robust
384 circadian rhythms of PER even under such fluctuation in activators, resulting in noisy
385 transcription of PER. For this, we simulated the TTFL model (Figure 1A), where the
386 activator level changes according to the experimentally measured BMAL1 (Figure 4A).
387 The amplitude of oscillation is highly variable with linear and ultrasensitive
388 phosphorylations (Figure 4B, green and blue). Furthermore, additional peaks in the
389 nuclear PER complex ($R_n$) are observed with linear and ultrasensitive phosphorylations.
390 In contrast, with bistable phosphorylation, robust rhythms with similar amplitudes are
391 generated (Figure 4B, red). Moreover, the additional peaks do not appear. As a result,

392 the CV of the peak-to-peak period and the amplitude are much smaller with bistable
393 phosphorylation than with linear and ultrasensitive phosphorylations (Figure 4C). Taken
394 together, bistable phosphorylation enables robust circadian rhythms despite fluctuation in
395 activator rhythms.

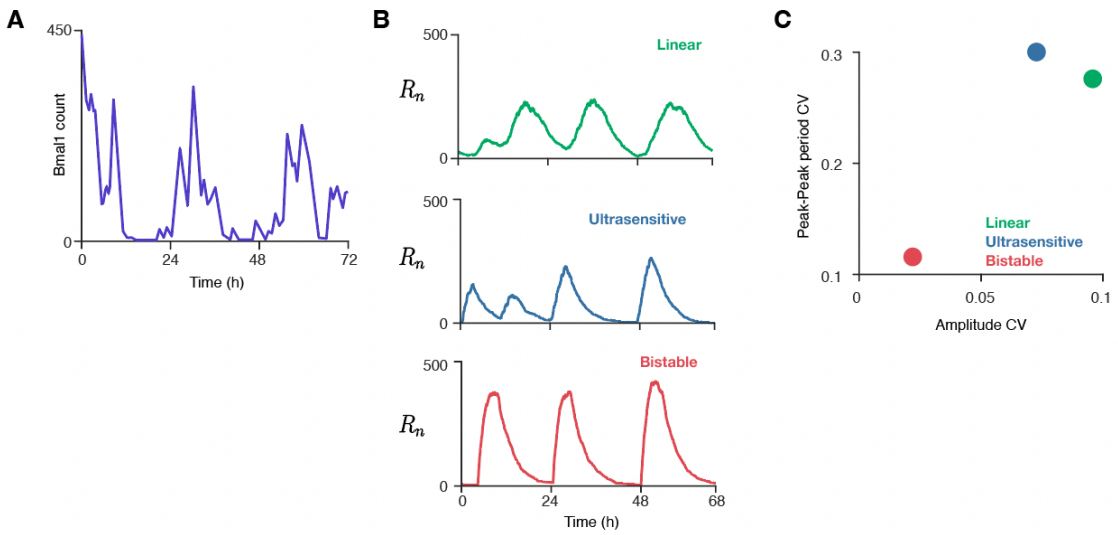


396

397 **Figure 4. Bistable phosphorylation enables cells to sustain robust circadian**
398 **rhythms even under noisy activator rhythms. (A)** The level of activator protein BMAL1
399 fluctuates across a day and exhibits daily change. In addition, an additional bump often
400 exists, resulting in more than one peak during a single cycle. The graph was retrieved
401 from Blanchoud et al.[14]. **(B)** Even with such noisy activator time series, bistable
402 phosphorylation leads to robust rhythms, unlike linear and ultrasensitive phosphorylations.
403 **(C)** As a result, the CV of both the peak-to-peak period and the amplitudes is small with
404 bistable phosphorylation, but not with linear and ultrasensitive phosphorylation.
405

406 # Discussion

407 For the TTFL to generate robust circadian rhythms, precise nucleus entry of the PER
408 complex is critical[7-10]. However, the distribution of the PER complex arrival time at the
409 perinuclear region is highly heterogeneous due to various noise sources. Despite this,
410 precise nucleus entry of the PER complex and transcriptional repression occur in the

411 circadian clock. To investigate the molecular mechanism underlying the unexpected
412 precision of the circadian clock, we constructed a mathematical model describing the
413 effect of protein arrival time on circadian rhythms (Figure 1A). We found that when the
414 protein arrival time varies due to the change of cytoplasmic congestion level, cell size,
415 and activator level, bistable phosphorylation, but not linear and ultrasensitive
416 phosphorylations, leads to precise repression timing, and thus robust circadian rhythms
417 (Figures 2-4). This indicates that the bistable phosphoswitch is the key mechanism to
418 filter the spatiotemporal noise in the cell to generate circadian rhythms. Spatiotemporally
419 regulated bistable phosphorylation can also play a critical role in other biological
420 oscillators, such as the cell cycle[54-56].

421 The mathematical model used in our study describes the spatiotemporal dynamics of
422 the TTFL of the circadian clock. In previous studies, the spatiotemporal dynamics of
423 molecules from the cytoplasm to the nucleus were directly described using PDE[33] or
424 agent-based models[8,32]. This approach was computationally expensive and not flexible
425 to describe the various noise sources for the protein arrival time of molecules to the
426 perinucleus. To describe the spatiotemporal dynamics of molecules simply and flexibly,
427 we used a travel time distribution as in previous studies, which described a chain of
428 signaling processes or protein synthesis[57-61]. Furthermore, it is challenging to model
429 ultrasensitive and bistable phosphorylations since they are generated from complex
430 combinations of multiple reactions. To resolve this, we utilized a modular approach that
431 describes those complex multistep reactions with a phenomenological module, which was
432 developed in work by De Boeck et al.[46]. This allowed us to effectively capture the key
433 dynamics of the phosphorylation mechanisms without comprehensively modeling the

underlying complex reactions. Using the distributed travel time and the modular approach are effective tools for describing complex intracellular spatiotemporal dynamics.

The nuclear entry of PER is delayed by the bistable phosphoswitch until a certain accumulation level is reached. Such delayed nuclear entry of PER has been observed in previous studies with *Drosophila* and mammals[8,62]. However, a study reported a rapid PER import when a protein synthesis inhibitor, cycloheximide (CHX), was applied and then removed from the cell[63]. The cause for the conflicting results observed in previous studies remains unclear, as the detailed mechanisms for nuclear entry and its rate constants have not been fully explored. One potential explanation is that CHX disrupts the phosphoswitch by inhibiting the synthesis of proteins, including kinase and phosphatase. Note that the balance between kinase and phosphatase is essential for the bistable phosphoswitch function[8,64]. To investigate the nuclear entry of PER regulated by the bistable phophoswitch, it is important to avoid perturbing the endogenous condition. This is also important for investigating the nuclear entry in biological systems other than the circadian clock. For example, in pancreatic $\beta$-cells, the nuclear entry of cPKA should be slow to distinguish the time scales of external signals[65]. While the underlying molecular mechanisms of such slow nuclear entry have not been known, the bistable phosphoswitch could be a potential molecular mechanism leading to such regulation of cPKA in pancreatic $\beta$-cells.

Alzheimer's disease (AD) has been reported to disrupt the circadian clock[66]. Such distribution appears to be due to tauopathy, which triggers the formation of neurofibrillary tangles, and thus increases cytoplasmic crowdedness[8]. However, even though tauopathy is one of the earliest events in AD development[67], the activity rhythms of mild symptomatic

457 dementia patients are not significantly different from those of non-patients[68,69]. This can
458 be explained by our results: the bistable phosphoswitch allows the circadian rhythms to
459 function normally up to a reasonable increase in intracellular congestion level.
460

461 ## Limitations of the study

462 In this work, we utilized an extension of the Gillespie algorithm to simulate the system
463 describing the TTFL. This allowed us to describe the effects of various noise sources on
464 circadian rhythms. To use the Gillespie algorithm for a system containing non-elementary
465 propensity functions (e.g., Hill functions) other than functions from mass-action kinetics,
466 timescale separation is necessary[70-72]. Thus, we assumed that the synthesis and the
467 degradation of PER are slower than other reactions, such as binding and unbinding of
468 PER to activator proteins and each step of its phosphorylation and dephosphorylation.
469 However, timescale separation is often not enough for accurate stochastic simulations,
470 unlike deterministic simulations; i.e., the condition for using the non-elementary
471 propensity functions for stochastic simulation is stricter than the deterministic
472 simulations[71,73-75]. Furthermore, the validity of using non-elementary propensity functions
473 for stochastic simulations in the presence of distributed delays has not been investigated,
474 which will be interesting in future work.

475 Clock proteins have complex interactions with each other. For example, BMAL1
476 regulates PER2 transcription, while PER2 regulates BMAL1 transcription by affecting the
477 transcription of REV-ERB and RORs, which are transcriptional regulators of BMAL1[4].
478 However, our model omits the regulation of BMAL1 by PER2 for simplicity in Figure 4.

Further work could include regulation from PER2 to BMAL1 and examining the interaction between the repressor proteins and activator proteins in the circadian clock.

Cell size keeps changing due to cell growth or cell division, which affects the TTFL of the circadian clock. Specifically, as cell size changes, the cytoplasmic trafficking of PER molecules changes, which is investigated in our study by using a time delay distribution (Figures 1F, 3A-3F). However, we did not investigate other critical factors, such as the dilution of the PER molecules during cell growth and their partition into daughter cells after cell division[76-78]. It would be interesting in future work to extend our study to incorporate dilution due to cell growth and the partition of molecules after cell division to investigate further the effect of the cell size changes on circadian rhythms.

## Acknowledgements

This work was supported by the Human Frontiers Science Program Organization (grant no. RGY0063/2017) (J.K.K.), the Institute for Basic Science (grant no. IBS-R029-C3) (J.K.K.), the Korea University Grant (S.L.) and the National Research Foundation of Korea (NRF) grant funded by the Korea government (MSIP) (No. 2020R1A2C1A01100114) (S.L).

## Author contributions

All authors designed the study. S.J.C. performed and D.W.K., S.L. and J.K.K. contributed to computational modeling and simulation. All authors analyzed the data. J.K.K.

supervised the project. S.J.C. and J.K.K. wrote the draft of the manuscript, and all authors revised the manuscript.

## Declaration of interests

The authors declare no competing interests.

## STAR★Methods

### RESOURCE AVAILABILITY

**Lead contact**

Further information and requests for resources and reagents should be directed to and will be fulfilled by the Lead Contact, Jae Kyoung Kim (jaekkim@kaist.ac.kr).

**Materials availability**

This study did not generate new unique reagents.

**Data and code availability**

- This paper analyzes publicly available existing data. These accession numbers for the datasets are listed in the key resources table.
- The MATLAB and Netlogo codes of the computational package are available in the following Database: The link will be available upon acceptance of the manuscript.
- Any additional information required to analyze the data is available from the lead contact upon request.

## METHODS DETAILS

**The stochastic model of the circadian clock simulating the TTFL with the spatiotemporal behavior of PER proteins.**

We extended a previous mathematical model of the mammalian circadian clock[19,21,22,28] to study the influence of the spatiotemporal behavior of PER proteins on circadian rhythms (see Tables S1 and S2 for detailed reactions and parameters used in the simulation). Specifically, our model consists of four variables: PER protein in the peripheral cytoplasm ($R_c$), unphosphorylated PER complex in the perinucleus ($R_p$), phosphorylated PER complex in the perinucleus ($R_p'$), and PER complex in the nucleus ($R_n$), which degrade with the same rate constant of $\lambda_d$.

In the model, $R_c$ is synthesized at the rate of $\lambda_p \max\left(1-\frac{R_n}{A}, 0\right)$, where $A$ is the number of activator proteins and $\lambda_p$ is the maximum synthesis rate. The synthesis rate is proportional to the fraction of free activator that is not sequestrated by PER complex in the nucleus, described by $\max\left(1-\frac{R_n}{A}, 0\right)$. This is an approximated form of the quasi-steady state of the fraction of free activators found by applying the total quasi-steady state approximation reduction to the detailed model describing the circadian clock[19,21,22,28] under the assumption that PER quickly binds and unbinds to the activator: $\frac{A-R_n-K_d\Omega+\sqrt{(A-R_n-K_d\Omega)^2+4AK_d\Omega}}{2A}$, where $K_d$ is the dissociation constant between the activator and PER, and $\Omega$ is the volume of the system. Then, by further assuming that the binding is tight ($K_d \to 0$), the fraction of free activator can be approximated by $\max(1-\frac{R_n}{A}, 0)$[19,21,22,28]. Up to Figure 3, $A$ was fixed to be 300, assuming the number of the activator is constant over time to focus on the spatiotemporal dynamics of PER. In Figure 4, to

545 investigate whether bistable phosphorylation enables robust circadian rhythms even
546 under noisy activator rhythms, we changed $A$ according to the experimentally measured
547 time series of BMAL1 molecules in a single cell[14]. From 72h-long experimentally
548 measured BMAL1 data, the first four hours were excluded to avoid the effect of the initial
549 shock for the experiment and then repeated to generate a long time series of $A$. Since the
550 experimentally measured BMAL1 time series was discrete, we linearly interpolated the
551 data to obtain the amount of BMAL1 in continuous time.

552 After being synthesized, $R_c$ passes through the cytoplasm crowded with obstacles
553 during a gamma-distributed travel time $\tau$. Specifically, when each $R_c$ molecule is
554 produced, $\tau$ is sampled from the gamma distribution and assigned to each molecule. Here,
555 the gamma distribution is utilized because it successfully captures the distribution of time
556 spent during the cytoplasmic trafficking. To determine the shape of the gamma
557 distribution, we utilized a previously proposed method using the ABM model, which
558 describes the cytoplasmic trafficking, so that the mean and the standard deviation of $\tau$
559 can be obtained (see Supplemental Information for details). When the experimentally
560 measured diffusion coefficient of PER of $0.2\mu m^2/s$[11,12] and the mean area of the fibroblast
561 cell of 2346$\mu m^2$ were used, the PDE simulation resulted in $\mu_\tau$=4.9h. This value of $\mu_\tau$ was
562 used in Figure 2 and Figure 4. $\sigma_\tau$ was set to be $\sigma_\tau = 0.5 \cdot \mu_\tau$ to ensure linear and
563 ultrasensitive phosphorylations to generate oscillations.

564 The PER complex that arrives at the perinucleus ($R_p$) undergoes phosphorylation
565 to be $R_p'$. Then, $R_p'$ is either dephosphorylated to $R_p$ with the rate of $\frac{1}{\tau_p}$ or enters the
566 nucleus with the rate of $\lambda_n$. To simply describe the phosphorylation based on multiple
567 reactions, we adopted the modular approach[46], which treated the phosphorylation

568 reaction as a single phenomenological module. That is, the module takes the total amount
569 of PER complex in the perinucleus ($T = R_p + R_p'$) as the input and gives the fraction of
570 the $R_p'$ in the perinucleus as the output. Among possible responses that the module can
571 generate, we chose linear phosphorylation, ultrasensitive phosphorylation, and bistable
572 phosphorylation[47]. With linear phosphorylation, the fraction of $R_p'$ ($= \frac{R_p'}{T}$) is constant
573 regardless of $T$ (Figure 2A, green). Such response is obtained by utilizing the propensity
574 function for the phosphorylation $f(T) = \frac{c \cdot T}{\tau_p}$, where $c$ is between 0 and 1. In our simulation,
575 the time scale of phosphorylation and dephosphorylation reactions, $\tau_p$, was set to be
576 sufficiently short ($\tau_p = \frac{1}{60}$h) so that the phosphorylation and dephosphorylation quickly
577 equilibrate (i.e., $\frac{c \cdot T}{\tau_p} = \frac{R_p'}{\tau_p}$). As a result, the fraction of $R_p'$ equilibrates to $\frac{R_p'}{T} = c$. Here, $c =$
578 $0.7$ was chosen to make the fraction of $R_p'$ be 70%. For ultrasensitive phosphorylation, the
579 fraction of $R_p'$ monotonically increases as $T$ increases, with a steep increase near the
580 threshold. To describe ultrasensitive phosphorylation, the propensity function $f(T) =$
581 $\frac{1}{\tau_p}\left(\frac{T^{n+1}}{T^n + K_u^n}\right)$ was used. Thus, the fraction of $R_p'$ ($\frac{R_p{}'}{T}$) quickly equilibrates to $\frac{T^n}{T^n + K_u^n}$, which was
582 used to describe the ultrasensitive response previously[43,46]. We set $K_u = 400$ and $n = 70$
583 to obtain a steep increase in the fraction of $R_p'$ when $T$ reaches $400$ (Figure 2A, blue). For
584 bistable phosphorylation, the response is bifurcating (i.e., the response qualitatively
585 varies depending on variables other than $T$), being affected by $R_p'$. Thus, the response of
586 bistable phosphorylation is described not only by $T$, but also by $R_p'$. To describe bistable
587 phosphorylation, we used an implicit function $f(T, R_p') = \frac{1}{\tau_p}\left(\frac{T^{m+1}}{T^m + \max(0.125 \cdot K_b, K_b - 5 \cdot R_p')^m}\right)$
588 after modifying a function generating an S-shaped response curve (i.e., bistable

589 response)[46]. $\frac{R_p'}{T}$ quickly equilibrates to $\frac{T^m}{T^m+\max(0.125\cdot K_b, K_b-5\cdot R_p')^m}$, which steeply increases

590 when $T$ increases to reach the switch-on threshold, $K_b$. Once $T$ reaches $K_b$, the fraction

591 of $R_p'$ stays near one even though $T$ decreases below $K_b$ until it reaches the switch-off

592 threshold, which is about $\frac{K_b}{8}$. Here, we chose $m = 30$ and $K_b = 400$ (Figure 2A, red).

593 The model was simulated using the delayed Gillespie algorithm[48,49]. For the

594 Gillespie simulation, the volume of the system was set to 1. See Tables S1 and S2 for

595 detailed descriptions of propensity functions and parameters used in the simulation,

596 respectively. In Figures 2B-2E and Figures 3B-3D, to focus on how the phosphorylation

597 affects the distribution of $t_n$, the synthesis of $R_c$ and the degradation of PER molecules

598 are excluded from the simulation. Specifically, we set $\lambda_p$ and $\lambda_d$ to be 0 to make these

599 reactions not occur. The initial condition was given by $R_c = 1000$, $R_p = R_p' = R_n = 0$.

600

601 ## QUANTIFICATIONS AND STATISTICAL ANALYSIS

602 **Quantification of features of the oscillation.**

603 We calculated several features (e.g., period, amplitude, correlation time) from the

604 oscillatory time series. First, in Figure 2G, we calculated the correlation time[50,51] and the

605 relative amplitude[31], as done in previous studies. Specifically, to calculate the correlation

606 time, we estimated parameters $\tau_C$ and $P$ by fitting $DC(s) = \exp\left(-\frac{s}{\tau_C}\right)\cdot\cos\left(\frac{2\pi s}{P}\right)$ to the

607 autocorrelation function $C(s) = \frac{\langle(x(t+s)-\langle x\rangle)(x(t)-\langle x\rangle)\rangle_s}{\langle x^2\rangle-\langle x\rangle^2}$ where $x(t)$ is the $R_n$ time series

608 obtained from the simulation. Then, the correlation time is defined as $\tau_C$, and it describes

609 how fast the autocorrelation decays over time. Thus, a more robust oscillation has a larger

610 $\tau_C$. The relative amplitude was calculated as the fraction of the amplitude (i.e., the

difference between the peak height and trough height of the given rhythms) to the peak height. To calculate the correlation time and the relative amplitude, the $R_n$ time series obtained from the simulation for 100 days (i.e., 2,400h) was used after the first 10 days were excluded to avoid the effect of transient dynamics. We repeated ten simulations with the same initial condition of having no PER molecule in the cell. Then, we took the average correlation time over ten repetitions.

In Figure 3A, we calculated the period of the oscillation by fitting the $C(s)$ to $DC(s)$ for simulated time series of $R_n$ for 100 days after excluding first 10 transient days. Then, we used the estimated $P$ as the period. We repeated this over ten different simulated trajectories and used the average of the estimated $P$ as the period.

To calculate the accumulation time of $R_n$ in Figure 3F and the peak-to-peak period in Figure 4, the time series of $R_n$ simulated for 100 days after excluding first 10 transient days was used. Then, the accumulation time of $R_n$ was measured from each cycle over 10 repeated simulations and then the mean of $R_n$ accumulation time was calculated. The peak-to-peak period was measured from each cycle over 10 repeated simulations, and then CV was calculated (Figure 4).

## KEY RESOURCE TABLE

| REAGENT or RESOURCE | SOURCE | IDENTIFIER |
|---|---|---|
| Software and algorithms | | |
| MATLAB R2021b | MathWorks | https://mathworks.com; RRID:SCR_001622 |
| Netlogo 3D 6.1.1 | CCL | https://ccl.northwestern.edu/netlogo/ |
| Others | | |
| Mouse fibroblast cell size data | Li et al.[40] | https://www.pnas.org/doi/full/10.1073/pnas.1922388117 |

| | | |
|---|---|---|
| BMAL1 time series data | Blanchoud et al.[14] | https://www.sciencedirect.com/science/article/abs/pii/S104620231500170X |

629

# References


1. Reppert, S.M., and Weaver, D.R. (2001). Molecular analysis of mammalian circadian rhythms. Annu Rev Physiol *63*, 647-676. https://doi.org/10.1146/annurev.physiol.63.1.647.
2. Ueda, H.R., Chen, W., Adachi, A., Wakamatsu, H., Hayashi, S., Takasugi, T., Nagano, M., Nakahama, K., Suzuki, Y., Sugano, S., et al. (2002). A transcription factor response element for gene expression during circadian night. Nature *418*, 534-539. 10.1038/nature00906.
3. Gallego, M., and Virshup, D.M. (2007). Post-translational modifications regulate the ticking of the circadian clock. Nat Rev Mol Cell Biol *8*, 139-148. https://doi.org/10.1038/nrm2106.
4. Takahashi, J.S. (2017). Transcriptional architecture of the mammalian circadian clock. Nat Rev Genet *18*, 164-179. https://doi.org/10.1038/nrg.2016.150.
5. Honma, S. (2018). The mammalian circadian system: a hierarchical multi-oscillator structure for generating circadian rhythm. J Physiol Sci *68*, 207-219. https://doi.org/10.1007/s12576-018-0597-5.
6. Cao, X., Yang, Y., Selby, C.P., Liu, Z., and Sancar, A. (2021). Molecular mechanism of the repressive phase of the mammalian circadian clock. Proc Natl Acad Sci U S A *118*. https://doi.org/10.1073/pnas.2021174118.
7. Tamanini, F., Yagita, K., Okamura, H., and van der Horst, G.T.J. (2005). Nucleocytoplasmic Shuttling of Clock Proteins. In Methods in Enzymology, M.W. Young, ed. (Academic Press), pp. 418-435. https://doi.org/10.1016/S0076-6879(05)93020-6.
8. Beesley, S., Kim, D.W., D'Alessandro, M., Jin, Y., Lee, K., Joo, H., Young, Y., Tomko, R.J., Faulkner, J., Gamsby, J., et al. (2020). Wake-sleep cycles are severely disrupted by diseases affecting cytoplasmic homeostasis. Proceedings of the National Academy of Sciences *117*, 28402-28411. https://doi.org/10.1073/pnas.2003524117.
9. Hurley, J.M. (2020). Cytoplasmic traffic jams affect circadian timing. Science Translational Medicine *12*, eabf4681. https://doi.org/10.1126/scitranslmed.abf4681.
10. Montague-Cardoso, K. (2020). Sleep-wake cycles are disrupted by diseases that result in cytoplasmic crowding. Communications Biology *3*, 705. https://doi.org/10.1038/s42003-020-01445-8.
11. Smyllie, N.J., Pilorz, V., Boyd, J., Meng, Q.J., Saer, B., Chesham, J.E., Maywood, E.S., Krogager, T.P., Spiller, D.G., Boot-Handford, R., et al. (2016). Visualizing and Quantifying Intracellular Behavior and Abundance of the Core Circadian Clock Protein PERIOD2. Curr Biol *26*, 1880-1886. https://doi.org/10.1016/j.cub.2016.05.018.
12. Koch, A.A., Bagnall, J.S., Smyllie, N.J., Begley, N., Adamson, A.D., Fribourgh, J.L., Spiller, D.G., Meng, Q.-J., Partch, C.L., Strimmer, K., et al. (2022). Quantification of protein abundance and interaction defines a mechanism for operation of the circadian clock. eLife *11*, e73976. https://doi.org/10.7554/eLife.73976.

13. Suter, D.M., Molina, N., Gatfield, D., Schneider, K., Schibler, U., and Naef, F. (2011). Mammalian genes are transcribed with widely different bursting kinetics. Science *332*, 472-474. https://doi.org/10.1126/science.1198817.
14. Blanchoud, S., Nicolas, D., Zoller, B., Tidin, O., and Naef, F. (2015). CAST: An automated segmentation and tracking tool for the analysis of transcriptional kinetics from single-cell time-lapse recordings. Methods *85*, 3-11. https://doi.org/10.1016/j.ymeth.2015.04.023.
15. Goldbeter, A. (1995). A model for circadian oscillations in the Drosophila period protein (PER). Proc Biol Sci *261*, 319-324. https://doi.org/10.1098/rspb.1995.0153.
16. Tyson, J.J., Hong, C.I., Thron, C.D., and Novak, B. (1999). A simple model of circadian rhythms based on dimerization and proteolysis of PER and TIM. Biophys J *77*, 2411-2417. https://doi.org/10.1016/S0006-3495(99)77078-5.
17. Forger, D.B., and Peskin, C.S. (2003). A detailed predictive model of the mammalian circadian clock. Proc Natl Acad Sci U S A *100*, 14806-14811. https://doi.org/10.1073/pnas.2036281100.
18. Leloup, J.C., and Goldbeter, A. (2003). Toward a detailed computational model for the mammalian circadian clock. Proc Natl Acad Sci U S A *100*, 7051-7056. https://doi.org/10.1073/pnas.1132112100.
19. Kim, J.K., and Forger, D.B. (2012). A mechanism for robust circadian timekeeping via stoichiometric balance. Mol Syst Biol *8*, 630. https://doi.org/10.1038/msb.2012.62.
20. Jolley, C.C., Ukai-Tadenuma, M., Perrin, D., and Ueda, H.R. (2014). A mammalian circadian clock model incorporating daytime expression elements. Biophys J *107*, 1462-1473. 10.1016/j.bpj.2014.07.022.
21. Kim, J.K., Kilpatrick, Z.P., Bennett, M.R., and Josic, K. (2014). Molecular mechanisms that regulate the coupled period of the mammalian circadian clock. Biophys J *106*, 2071-2081. https://doi.org/10.1016/j.bpj.2014.02.039.
22. Kim, J.K. (2016). Protein sequestration versus Hill-type repression in circadian clock models. IET Syst Biol *10*, 125-135. https://doi.org/10.1049/iet-syb.2015.0090.
23. Wang, Y., Ni, X., Yan, J., and Yang, L. (2017). Modeling transcriptional co-regulation of mammalian circadian clock. Math Biosci Eng *14*, 1447-1462. https://doi.org/10.3934/mbe.2017075.
24. Abel, J.H., Chakrabarty, A., Klerman, E.B., and Doyle, F.J., 3rd (2019). Pharmaceutical-based entrainment of circadian phase via nonlinear model predictive control. Automatica (Oxf) *100*, 336-348. https://doi.org/10.1016/j.automatica.2018.11.012.
25. Del Olmo, M., Kramer, A., and Herzel, H. (2019). A Robust Model for Circadian Redox Oscillations. Int J Mol Sci *20*. https://doi.org/10.3390/ijms20092368.
26. Kim, D.W., Chang, C., Chen, X., Doran, A.C., Gaudreault, F., Wager, T., DeMarco, G.J., and Kim, J.K. (2019). Systems approach reveals photosensitivity and PER2 level as determinants of clock-modulator efficacy. Mol Syst Biol *15*, e8838. https://doi.org/10.15252/msb.20198838.

27. Breitenbach, T., Helfrich-Forster, C., and Dandekar, T. (2021). An effective model of endogenous clocks and external stimuli determining circadian rhythms. Sci Rep *11*, 16165. https://doi.org/10.1038/s41598-021-95391-y.
28. Kim, J.K. (2021). Tick, Tock, Circadian Clocks. In Case Studies in Systems Biology, P. Kraikivski, ed. (Springer International Publishing), pp. 79-94. https://doi.org/10.1007/978-3-030-67742-8_6.
29. Kim, R., and Reed, M.C. (2021). A mathematical model of circadian rhythms and dopamine. Theor Biol Med Model *18*, 8. https://doi.org/10.1186/s12976-021-00139-w.
30. Mosig, R.A., Castaneda, A.N., Deslauriers, J.C., Frazier, L.P., He, K.L., Maghzian, N., Pokharel, A., Schrier, C.T., Zhu, L., Koike, N., et al. (2021). Natural antisense transcript of Period2, Per2AS, regulates the amplitude of the mouse circadian clock. Genes Dev *35*, 899-913. https://doi.org/10.1101/gad.343541.120.
31. Jeong, E.M., Kwon, M., Cho, E., Lee, S.H., Kim, H., Kim, E.Y., and Kim, J.K. (2022). Systematic modeling-driven experiments identify distinct molecular clockworks underlying hierarchically organized pacemaker neurons. Proceedings of the National Academy of Sciences *119*, e2113403119. https://doi.org/doi:10.1073/pnas.2113403119.
32. Sturrock, M., Hellander, A., Matzavinos, A., and Chaplain, M.A. (2013). Spatial stochastic modelling of the Hes1 gene regulatory network: intrinsic noise can explain heterogeneity in embryonic stem cell differentiation. J R Soc Interface *10*, 20120988. https://doi.org/10.1098/rsif.2012.0988.
33. Ma, J., Do, M., Le Gros, M.A., Peskin, C.S., Larabell, C.A., Mori, Y., and Isaacson, S.A. (2020). Strong intracellular signal inactivation produces sharper and more robust signaling from cell membrane to nucleus. PLOS Computational Biology *16*, e1008356. https://doi.org/10.1371/journal.pcbi.1008356.
34. Chen, W., Smeekens, J.M., and Wu, R. (2016). Systematic study of the dynamics and half-lives of newly synthesized proteins in human cells. Chem Sci *7*, 1393-1400. https://doi.org/10.1039/c5sc03826j.
35. Lee, C., Etchegaray, J.P., Cagampang, F.R., Loudon, A.S., and Reppert, S.M. (2001). Posttranslational mechanisms regulate the mammalian circadian clock. Cell *107*, 855-867. https://doi.org/10.1016/s0092-8674(01)00610-9.
36. Isojima, Y., Nakajima, M., Ukai, H., Fujishima, H., Yamada, R.G., Masumoto, K.H., Kiuchi, R., Ishida, M., Ukai-Tadenuma, M., Minami, Y., et al. (2009). CKIepsilon/delta-dependent phosphorylation is a temperature-insensitive, period-determining process in the mammalian circadian clock. Proc Natl Acad Sci U S A *106*, 15744-15749. 10.1073/pnas.0908733106.
37. Zhou, M., Kim, J.K., Eng, G.W., Forger, D.B., and Virshup, D.M. (2015). A Period2 Phosphoswitch Regulates and Temperature Compensates Circadian Period. Mol Cell *60*, 77-88. https://doi.org/10.1016/j.molcel.2015.08.022.
38. Narasimamurthy, R., Hunt, S.R., Lu, Y., Fustin, J.M., Okamura, H., Partch, C.L., Forger, D.B., Kim, J.K., and Virshup, D.M. (2018). CK1delta/epsilon protein kinase primes the PER2 circadian phosphoswitch. Proc Natl Acad Sci U S A *115*, 5986-5991. https://doi.org/10.1073/pnas.1721076115.

39. Masuda, S., Narasimamurthy, R., Yoshitane, H., Kim, J.K., Fukada, Y., and Virshup, D.M. (2020). Mutation of a PER2 phosphodegron perturbs the circadian phosphoswitch. Proc Natl Acad Sci U S A *117*, 10888-10896. https://doi.org/10.1073/pnas.2000266117.
40. Li, Y., Shan, Y., Desai, R.V., Cox, K.H., Weinberger, L.S., and Takahashi, J.S. (2020). Noise-driven cellular heterogeneity in circadian periodicity. Proc Natl Acad Sci U S A *117*, 10350-10356. https://doi.org/10.1073/pnas.1922388117.
41. Novak, B., and Tyson, J.J. (2008). Design principles of biochemical oscillators. Nat Rev Mol Cell Biol *9*, 981-991. https://doi.org/10.1038/nrm2530.
42. Ferrell, James E., Jr., Tsai, Tony Y.-C., and Yang, Q. (2011). Modeling the Cell Cycle: Why Do Certain Circuits Oscillate? Cell *144*, 874-885. 10.1016/j.cell.2011.03.006.
43. Ferrell, J.E., Jr., and Ha, S.H. (2014). Ultrasensitivity part II: multisite phosphorylation, stoichiometric inhibitors, and positive feedback. Trends Biochem Sci *39*, 556-569. https://doi.org/10.1016/j.tibs.2014.09.003.
44. Lee, H., Chen, R., Lee, Y., Yoo, S., and Lee, C. (2009). Essential roles of CKIdelta and CKIepsilon in the mammalian circadian clock. Proc Natl Acad Sci U S A *106*, 21359-21364. https://doi.org/10.1073/pnas.0906651106.
45. Narasimamurthy, R., and Virshup, D.M. (2021). The phosphorylation switch that regulates ticking of the circadian clock. Molecular Cell *81*, 1133-1146. https://doi.org/10.1016/j.molcel.2021.01.006.
46. De Boeck, J., Rombouts, J., and Gelens, L. (2021). A modular approach for modeling the cell cycle based on functional response curves. PLoS Comput Biol *17*, e1009008. https://doi.org/10.1371/journal.pcbi.1009008.
47. Tyson, J.J., and Novak, B. (2020). A Dynamical Paradigm for Molecular Cell Biology. Trends Cell Biol *30*, 504-515. https://doi.org/10.1016/j.tcb.2020.04.002.
48. Cai, X. (2007). Exact stochastic simulation of coupled chemical reactions with delays. J Chem Phys *126*, 124108. https://doi.org/10.1063/1.2710253.
49. Josic, K., Lopez, J.M., Ott, W., Shiau, L., and Bennett, M.R. (2011). Stochastic delay accelerates signaling in gene networks. PLoS Comput Biol *7*, e1002264. https://doi.org/10.1371/journal.pcbi.1002264.
50. Cao, Y., Wang, H., Ouyang, Q., and Tu, Y. (2015). The free energy cost of accurate biochemical oscillations. Nat Phys *11*, 772-778. https://doi.org/10.1038/nphys3412.
51. Qiao, L., Zhang, Z.-B., Zhao, W., Wei, P., and Zhang, L. (2021). Network design principle for robust oscillatory behaviors with respect to biological noise. bioRxiv, 2021.2012.2022.473835. https://doi.org/10.1101/2021.12.22.473835.
52. Rombouts, J., Vandervelde, A., and Gelens, L. (2018). Delay models for the early embryonic cell cycle oscillator. PLoS One *13*, e0194769. https://doi.org/10.1371/journal.pone.0194769.
53. Abe, Y.O., Yoshitane, H., Kim, D.W., Kawakami, S., Koebis, M., Nakao, K., Aiba, A., Kim, J.K., and Fukada, Y. (2022). Rhythmic transcription of Bmal1 stabilizes the circadian timekeeping system in mammals. Nat Commun *13*, 4652. https://doi.org/10.1038/s41467-022-32326-9.

807 54. Nomura, M., and Okada-Hatakeyama, M. (2013). Phase responses of oscillating
808 components in a signaling pathway. Front Physiol *4*, 68.
809 10.3389/fphys.2013.00068.
810 55. Gelens, L., Qian, J., Bollen, M., and Saurin, A.T. (2018). The Importance of
811 Kinase-Phosphatase Integration: Lessons from Mitosis. Trends Cell Biol *28*, 6-
812 21. 10.1016/j.tcb.2017.09.005.
813 56. Jin, M., Tavella, F., Wang, S., and Yang, Q. (2022). In vitro cell cycle oscillations
814 exhibit a robust and hysteretic response to changes in cytoplasmic density. Proc
815 Natl Acad Sci U S A *119*. 10.1073/pnas.2109547119.
816 57. Barrio, M., Leier, A., and Marquez-Lago, T.T. (2013). Reduction of chemical
817 reaction networks through delay distributions. J Chem Phys *138*, 104114.
818 https://doi.org/10.1063/1.4793982.
819 58. Park, S.J., Song, S., Yang, G.S., Kim, P.M., Yoon, S., Kim, J.H., and Sung, J.
820 (2018). The Chemical Fluctuation Theorem governing gene expression. Nat
821 Commun *9*, 297. https://doi.org/10.1038/s41467-017-02737-0.
822 59. Thurley, K., Wu, L.F., and Altschuler, S.J. (2018). Modeling Cell-to-Cell
823 Communication Networks Using Response-Time Distributions. Cell Syst *6*, 355-
824 367 e355. 10.1016/j.cels.2018.01.016.
825 60. Choi, B., Cheng, Y.Y., Cinar, S., Ott, W., Bennett, M.R., Josic, K., and Kim, J.K.
826 (2020). Bayesian inference of distributed time delay in transcriptional and
827 translational regulation. Bioinformatics *36*, 586-593.
828 https://doi.org/10.1093/bioinformatics/btz574.
829 61. Kim, D.W., Hong, H., and Kim, J.K. (2022). Systematic inference identifies a
830 major source of heterogeneity in cell signaling dynamics: The rate-limiting step
831 number. Sci Adv *8*. https://doi.org/10.1126/sciadv.abl4598.
832 62. Meyer, P., Saez, L., and Young, M.W. (2006). PER-TIM interactions in living
833 Drosophila cells: an interval timer for the circadian clock. Science *311*, 226-229.
834 10.1126/science.1118126.
835 63. Vanselow, K., Vanselow, J.T., Westermark, P.O., Reischl, S., Maier, B., Korte,
836 T., Herrmann, A., Herzel, H., Schlosser, A., and Kramer, A. (2006). Differential
837 effects of PER2 phosphorylation: molecular basis for the human familial
838 advanced sleep phase syndrome (FASPS). Genes Dev *20*, 2660-2672.
839 10.1101/gad.397006.
840 64. Park, J., Lee, K., Kim, H., Shin, H., and Lee, C. (2023). Endogenous circadian
841 reporters reveal functional differences of PERIOD paralogs and the significance
842 of PERIOD:CK1 stable interaction. Proc Natl Acad Sci U S A *120*, e2212255120.
843 10.1073/pnas.2212255120.
844 65. Peercy, B.E., and Sherman, A.S. (2010). How Pancreatic β-Cells Discriminate
845 Long and Short Timescale cAMP Signals. Biophysical Journal *99*, 398-406.
846 https://doi.org/10.1016/j.bpj.2010.04.043.
847 66. Stevanovic, K., Yunus, A., Joly-Amado, A., Gordon, M., Morgan, D., Gulick, D.,
848 and Gamsby, J. (2017). Disruption of normal circadian clock function in a mouse
849 model of tauopathy. Exp Neurol *294*, 58-67.
850 https://doi.org/10.1016/j.expneurol.2017.04.015.
851 67. Mondragon-Rodriguez, S., Perry, G., Luna-Munoz, J., Acevedo-Aquino, M.C.,
852 and Williams, S. (2014). Phosphorylation of tau protein at sites Ser(396-404) is

one of the earliest events in Alzheimer's disease and Down syndrome. Neuropathol Appl Neurobiol *40*, 121-135. https://doi.org/10.1111/nan.12084.

68. Hatfield, C.F., Herbert, J., van Someren, E.J., Hodges, J.R., and Hastings, M.H. (2004). Disrupted daily activity/rest cycles in relation to daily cortisol rhythms of home-dwelling patients with early Alzheimer's dementia. Brain *127*, 1061-1074. https://doi.org/10.1093/brain/awh129.
69. Musiek, E.S. (2017). Circadian Rhythms in AD pathogenesis: A Critical Appraisal. Curr Sleep Med Rep *3*, 85-92. https://doi.org/10.1007/s40675-017-0072-5.
70. Kim, J.K., Josić, K., and Bennett, M.R. (2015). The relationship between stochastic and deterministic quasi-steady state approximations. BMC Systems Biology *9*, 87. https://doi.org/10.1186/s12918-015-0218-3.
71. Song, Y.M., Hong, H., and Kim, J.K. (2021). Universally valid reduction of multiscale stochastic biochemical systems using simple non-elementary propensities. PLoS Comput Biol *17*, e1008952. https://doi.org/10.1371/journal.pcbi.1008952.
72. Kim, J.K., and Tyson, J.J. (2020). Misuse of the Michaelis-Menten rate law for protein interaction networks and its remedy. PLoS Comput Biol *16*, e1008258. https://doi.org/10.1371/journal.pcbi.1008258.
73. Thomas, P., Straube, A.V., and Grima, R. (2012). The slow-scale linear noise approximation: an accurate, reduced stochastic description of biochemical networks under timescale separation conditions. BMC Syst Biol *6*, 39. https://doi.org/10.1186/1752-0509-6-39.
74. Kim, J.K., Josić, K., and Bennett, M.R. (2014). The Validity of Quasi-Steady-State Approximations in Discrete Stochastic Simulations. Biophysical Journal *107*, 783-793. https://doi.org/10.1016/j.bpj.2014.06.012.
75. Kim, J.K., and Sontag, E.D. (2017). Reduction of multiscale stochastic biochemical reaction networks using exact moment derivation. PLoS Comput Biol *13*, e1005571. https://doi.org/10.1371/journal.pcbi.1005571.
76. Gonze, D. (2013). Modeling the effect of cell division on genetic oscillators. Journal of Theoretical Biology *325*, 22-33. https://doi.org/10.1016/j.jtbi.2013.02.001.
77. Veliz-Cuba, A., Hirning, A.J., Atanas, A.A., Hussain, F., Vancia, F., Josić, K., and Bennett, M.R. (2015). Sources of Variability in a Synthetic Gene Oscillator. PLOS Computational Biology *11*, e1004674. https://doi.org/10.1371/journal.pcbi.1004674.
78. Paijmans, J., Lubensky, D.K., and Rein Ten Wolde, P. (2017). Robustness of synthetic oscillators in growing and dividing cells. Phys Rev E *95*, 052403. https://doi.org/10.1103/PhysRevE.95.052403.